ELSEVIER

Desalination 190 (2006) 189–200

DESALINATION

www.elsevier.com/locate/desal

Modeling remineralization of desalinated water by limestone dissolution

David Hasson*, Orly Bendrihem

GWRI Rabin Desalination Laboratory, Department of Chemical Engineering, Technion — Israel Institute of Technology, Haifa, Israel
Tel. +972 (4) 8292936; Fax +972 (4) 8295672; email: hasson@techunix.technion.ac.il

Received 28 March 2005; accepted 15 September 2005

Abstract

Desalted waters or highly soft waters produced by desalination plants cannot be directly used as they are unpalatable, corrosive and unhealthy. Remineralization is necessary in order to overcome these problems. A commonly used operation in the remineralization process is to contact CO_2 acidified desalinated water with a bed of domestic limestone. Limestone dissolution provides two essential ingredients to the water — bicarbonate alkalinity and calcium content: $CaCO_3 + CO_2 + H_2O = Ca^{2+} + 2HCO_3^-$. Limestone dissolution is a slow rate-controlling step. Prediction of the limestone rate of dissolution as a function of the water composition is essential for reliable design and operation of the limestone contactor. A critical comparison of various kinetic expressions proposed in the literature carried out in this study reveals major differences in results evaluated from different dissolution models. An experimental study was conducted in order to identify the most reliable kinetic dissolution model. Two series of experiments were carried out — one involving remineralization of distilled water containing low initial CO_2 concentrations (0.5–2 mM) and the other, remineralization of soft water, having high initial CO_2 concentrations (1.5–15 mM). The CO_2 acidified water was contacted in a 2 m high vertical column (32 mm I.D.), packed with 2.85 mm calcite particles. The change in water composition along the column was monitored to provide both differential and integral dissolution data. Analysis of the data showed that none of the available models fitted the experimental results. The closest agreement was with the rather complex model of Plummer et al but this agreement was rather mediocre. In the high CO_2 content range, the model predicted dissolution rates higher by a factor of 2–4 in the high CO_2 range and by a factor of 10–20 in the low CO_2 range. Based on the experimental results, two models were developed for the design of limestone dissolution column contactors. When the final composition of the remineralized water has a CO_2 content above 2 mM, the limestone bed can be designed by a very simple integral

*Corresponding author.

Presented at the International Desalination Association World Congress on Desalination and Water Reuse, Paradise Island, Bahamas, 28 September – 3 October 2003.

0011-9164/06/$– See front matter
doi:10.1016/j.desal.2005.09.003

expression. However, if the dissolution depletes the CO_2 concentration to low values, well below 2 mM, the bed design requires numerical integration of the more general dissolution rate expression derived in this work.

Keywords: Post-treatment; Desalinated water stabilization; Limestone dissolution; Limestone bed design

1. Introduction

The lack of dissolved minerals in the high-purity waters produced by desalination processes raises some problems. High-purity water tends to be highly reactive and unless treated, it can create severe corrosion difficulties during its transport in conventional pipelines. For example, the cement mortar lining of water pipes deteriorates by the corrosive attack of soft waters. Also, untreated desalinated water cannot be used directly as a source of drinking water. A certain degree of re-mineralization is necessary in order to make the water palatable and for re-introducing some essential ions required from health considerations. According to Gabbrielli and Gerofi [1], the optimal ranges of TDS, hardness and specific ion content of remineralized water in mg/L are 200–400 for TDS, 50–75 for Ca, 0–10 for Mg, 0–100 for Na, 30–150 for Cl and 0–200 for sulfate — all units are in mg/L. The bicarbonate content recommendation is to have a concentration equivalent to the hardness content.

The main processes for the remineralization of desalinated water are as follows:

A. Dosage of chemical solutions (based on calcium chloride and sodium bicarbonate).
   Large-scale preparation and dosage of such mineralizing solutions is costly and impractical. This remineralization method is a viable option only for small-capacity plants.

B. Lime dissolution by carbon dioxide.
   This process involves treatment of milk of lime with CO_2 acidified desalinated water. The reaction involved is:

$$Ca(OH)_2 + 2CO_2 \rightarrow Ca^{2+} + 2HCO_3^- \quad (1)$$

C. Limestone dissolution by carbon dioxide.
   Contacting limestone with CO_2 acidified desalinated water mineralizes the solution according to:

$$CaCO_3 + CO_2 + H_2O \rightarrow Ca^{2+} + 2HCO_3^- \quad (2)$$

Limestone dissolution is the simplest and most widely used process. Limestone is cheaper than lime and half the CO_2 amount is consumed in the formation of the same minerals. Moreover, the equipment for handling limestone is much cheaper compared with the system required for preparing and dosing lime slurries. The only advantage of the lime process is that the reaction proceeds almost to completion whereas in the limestone process, the reaction is much slower and does not reach completion so that residual excess CO_2 has to be neutralized by addition of NaOH or Na_2CO_3. In large capacity plants, it is more economical to recover the excess CO_2 by degasification.

A difficulty in the design of limestone dissolution beds is the lack of reliable data on the kinetics of dissolution of limestone by CO_2 acidified water. The objective of the present study was to measure dissolution rates in a well controlled laboratory system and to confront the experimental data with the conflicting kinetic expressions published in the literature.

2. Characterization of the dissolution process

2.1. Thermodynamic equilibria

The solubility in water, $[CO_2]$ mol/L, of carbon dioxide in contact with a gaseous atmosphere having a partial pressure p_{CO_2} is dictated by Henry's law:

$$p_{CO_2} = H \times [CO_2] \quad (3)$$

The equilibrium maintained in solution by the various carbonate species is given by:

$$CO_2 + H_2O \rightleftharpoons H_2CO_3 \rightleftharpoons H^+ + \begin{matrix} HCO_3^- \\ \downarrow\uparrow \\ H^+ + CO_3^{2-} \end{matrix} \quad (4)$$

The total concentration of the carbonate species maintained in solution is:

$$C_T = CO_2 + HCO_3^- + CO_3^{2-} \quad (5)$$

The distribution of the species is governed by the first and second dissociation equilibria of carbonic acid:

$$[H^+] \times [HCO_3^-]/[CO_2] = K_1' \quad (6)$$

$$[H^+] \times [CO_3^{2-}]/[HCO_3^-] = K_2' \quad (7)$$

where K_1' and K_2' are the dissociation constants, adjusted for the ionic strength of the solution. The water dissociation equilibrium is given by:

$$[H^+] \times [OH^-] = K_w' \quad (8)$$

Eqs. (5)–(7) show that the carbonate species distribution is governed by the pH (Fig. 1). Note that at the pH range of about 4.5 to 8.5, which is of practical interest for water remineralization, the CO_3^{2-} concentration is negligibly small and only the CO_2 and HCO_3^- species need be considered.

Dissolution of limestone requires that the water composition be such that:

$$[Ca^{2+}] \times [CO_3^{2-}] < K_{sp}' \quad (9)$$

where K_{sp}' is the solubility product of the limestone crystals. The stable crystallographic form of limestone is calcite.

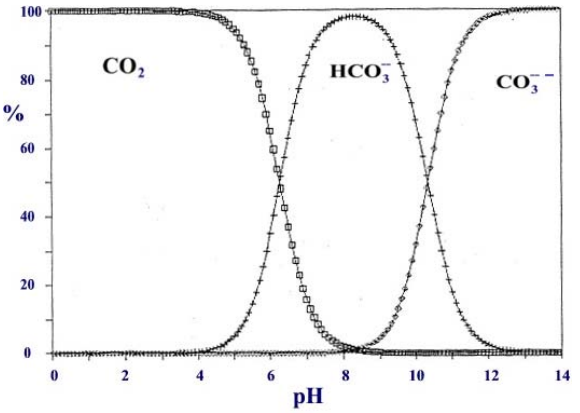

Fig. 1. Distribution of carbonate species at 25°C.

2.2. Dissolution path in a closed system

A closed system consists of a single phase liquid solution, not in contact with a gaseous phase. Here, the CO_2 concentration is depleted by the dissolution reaction [Eq. (2)]. The changes in solution composition accompanying dissolution are constrained by material and electric balances. Let the initial known composition of an aggressive water be denoted by $[Ca]_0$, $[CO_2]_0$, $[HCO_3]_0$, $[CO_3]_0$, $[H^+]_0$, $[OH^-]_0$.

The change in the concentration of each species is denoted by: $\Delta = C - C_0$, where C is a final condition. The mass balance constraint shows that:

$$\Delta[Ca] = \Delta[C_T] = \Delta[CO_2] + \Delta[HCO_3] + \Delta[CO_3] \cong \Delta[CO_2] + \Delta[HCO_3] \quad (10)$$

The electrical balance shows that:

$$2\Delta[Ca] = \Delta[HCO_3] + 2\Delta[CO_3] + \Delta[OH^-] - \Delta[H^+] \cong \Delta[HCO_3] \quad (11)$$

Combining Eqs. (10) and (11), it is seen that:

$$\Delta[Ca] = 1/2\Delta[HCO_3] = -\Delta[CO_2] \quad (12)$$

Thus, in the usual situation of negligibly small concentrations of the carbonate, hydrogen and hydroxyl ions, the dissolution path can be conveniently described (Fig. 2) by a simple linear relation between $[CO_2]$ and $[HCO_3]$ having a slope of –(1/2):

$$[CO_2] = \{[CO_2]_0 + [HCO_3]_0\} - 1/2[HCO_3] \quad (13)$$

The Ca concentration is linearly related to the HCO_3 concentration by:

$$[Ca] = 1/2[HCO_3] + \{[Ca]_0 - 1/2[HCO_3]_0\} \quad (14)$$

Inspection of the above system shows that in a dissolution process there are 6 unknown concentrations {[Ca], $[CO_2]$, $[HCO_3]$, $[CO_3]$, $[H^+]$, $[OH^-]$} and 5 equations [Eqs. (6)–(8), (13) and (14)]. Thus in order to follow composition changes occurring in a remineralization process, it is sufficient to measure only one of the six concentrations. The other 5 concentrations are readily determined by solution of the set of equilibria and balance constraints.

2.3. Dissolution in an open system

In an open system, in which there is a gaseous atmosphere held at a constant CO_2 partial pressure, the dissolved CO_2 concentration is constant. Here the total carbon in the dissolution path is not constant and replaces the CO_2 concentrations as an unknown variable. Dissolution acts to increase the pH of the solution. In the widely used pH-stat technique [2] for studying the kinetics of $CaCO_3$ dissolution, the pH is held constant by automatic acid titration which neutralizes the alkalinity increase accompanying dissolution. Under these conditions, all the parameters affecting the rate of dissolution are constant and the rate of acid dosage represents the rate of dissolution corresponding to the solution composition.

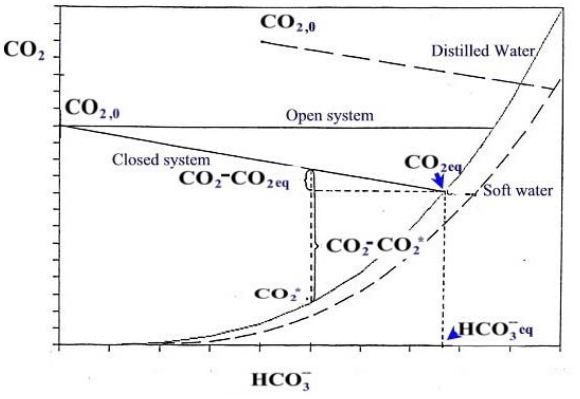

Fig. 2. Graphical illustration of dissolution paths and dissolution driving forces.

2.4. Terminal equilibrium composition

The dissolution process in a closed system terminates when the system reaches equilibrium conditions, characterized by:

$$[Ca^{2+}]_e \times [CO_3^{2-}]_e = K'_{sp} \quad (15)$$

where the subscript *e* denotes equilibrium conditions. Eliminating the CO_3 concentration from Eqs. (6), (7):

$$[CO_2]_e = \frac{K'_2}{K'_1 \cdot K'_{sp}} \cdot \{[Ca]_e \cdot [HCO_3]_e^2\} \quad (16)$$

Denoting the final conversion by $X = \Delta[Ca]$, the amount of Ca released by dissolution is given by

$$\frac{\{[Ca]_0 + X\} \cdot \{[HCO_3]_0 + 2X\}}{\{[CO_2]_0 - X\}} = \frac{K'_{sp} \cdot K'_1}{K'_2} \quad (17)$$

The final carbon species equilibrium concentrations, obtained in limestone dissolution of soft water containing some initial calcium bicarbonate, are related by:

$$[CO_2]_e = \frac{K'_2}{2K'_1 \cdot K'_{sp}} \cdot [HCO_3]_e^3 \cdot \left\{1 - \frac{[HCO_3]_0 - 2[Ca]_0}{[HCO_3]_e}\right\} \quad (18)$$

If dissolution occurs in distilled water, or in soft waters in which $\{2[Ca]_o = [HCO_3]_o\}$ the equilibrium concentrations are related by:

$$[CO_2]_e = \frac{K_2'}{2K_1' \cdot K_{sp}'} \cdot [HCO_3]_e^3 \quad (19)$$

Fig. 2 depicts graphically the dissolution path with CO_2 and HCO_3 coordinates. For a closed system, the dissolution path is the "operating line" of slope of –(1/2), given by Eq. (13). Plots of the $[CO_2]_e$ – $[HCO_3]_e$ equilibria, expressed by Eqs. (18), (19), are also shown. The intersection of the dissolution line with the equilibrium curve indicates the final equilibrium composition achieved in the system.

The driving force for the dissolution process is a difference between the actual water composition and its final equilibrium solubility. Fig. 2 illustrates two different driving forces that have been used in the literature in the development of kinetic expressions:

- Driving force based on the equilibrium CO_2 concentration: $[CO_2] – [CO_2]_e$
- Driving force based on a pseudo-equilibrium CO_2 concentration: $[CO_2] – [CO_2]^*$

The pseudo-equilibrium concentration $[CO_2]^*$ is an equilibrium concentration based on the prevailing Ca and HCO_3 concentrations:

$$[CO_2]^* = \frac{K_2'}{K_1' \cdot K_{sp}'} \cdot \{[Ca] \cdot [HCO_3]\} \quad (20)$$

3. Review of dissolution models

Table 1 summarizes the main features of various dissolution kinetic studies. Only papers dealing with dissolution of calcite in the absence of metallic impurities are considered here. Commonly encountered metallic impurities such as Zn^{2+} and Cu^{2+} can slow down significantly the dissolution of limestone. Available data on the effect of metallic impurities will be reviewed in a future publication.

As illustrated below, there are considerable differences in the experimental set-ups, in the methods adopted for measuring the dissolution rate and in the models used for correlating the dissolution rate data. The different dissolution paths in the various investigations are displayed in Fig. 3. Open systems, in which dissolution of powdered $CaCO_3$ particles occurred in the presence of a

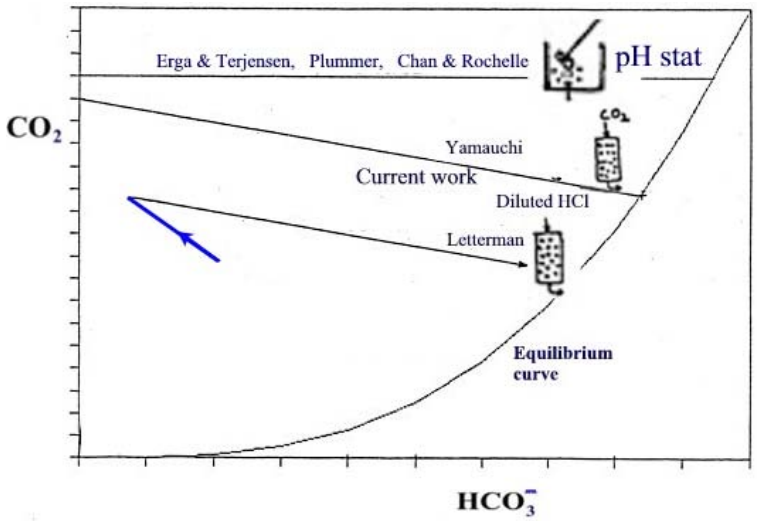

Fig. 3. Dissolution systems investigated in various studies.

Table 1
Summary of limestone dissolution rate studies

Authors	System	Dissolution rate expressions
Erga and Terjesen (1956) [3]	Dissolution of 0.3–0.4 mm $CaCO_3$ powder in stirred vessel in contact with constant pressure CO_2 gas at 25°C Initial solution — distilled water $[CO_2]_o$ = 9–60 mM Rate determined by free drift expts.	Mass transfer resistance neglected $R = k \cdot [\mathrm{Ca}]_e \cdot \{[\mathrm{Ca}]_e - [\mathrm{Ca}]\}$ $= k' \cdot [\mathrm{HCO_3}]_e \cdot \{[\mathrm{CO_2}] - [\mathrm{CO_2}]_e\}$
Plummer et al. (1978, 1979) [4,5]	Dissolution of 0.3–0.6 mm $CaCO_3$ powder in stirred vessel in contact with constant pressure CO_2 gas at temperatures of 5–60°C Initial solution — distilled water $[CO_2]_o$ = 0–60 mM Dissolution rates determined by both free drift and pH-stat expts.	Mass transfer resistance neglected Dissolution occurs by 3 simultaneous reactions involving attacks by H^+, CO_2 and H_2O. The CO_2 rate expression is: $R_2 = k \cdot [\mathrm{CO_2}] - k' \cdot \{[\mathrm{Ca}][\mathrm{HCO_3}][\mathrm{HCO_3}]_s\}$ where $[HCO_3]_s$ is the adsorbed surface concentration, assumed to be at equilibrium with bulk CO_2 concentration
Chan and Rochelle (1982) [6]	Dissolution of 0.01 mm $CaCO_3$ powder in stirred vessel in contact with constant pressure CO_2 gas at temperatures of 25 and 55°C Initial solution — 100 mM $CaCl_2$ $[CO_2]_o$ = 0–60 mM Dissolution rate determined by pH-stat expts.	Limited experimental data. Dissolution assumed to be controlled by mass transfer and not by surface reactions. Dissociation of carbonic acid is considered to be a slow rate controlling reaction given by: $R = k \cdot [\mathrm{CO_2}] - k' \cdot \{[\mathrm{HCO_3}][\mathrm{H^+}]\}$
Yamuchi et al. (1987) [7]	Dissolution by flow of CO_2 acidified distilled water at 40°C in a 100 mm diameter column, packed with $CaCO_3$ particles Packing length = 0.5–2.4 m Particle sizes = 1.4–10 mm $[CO_2]_o$ = 2.4–5 mM Superficial velocity = 2.5–9 mm/s Retention time = 55–270 s	Dissolution rate expression: $R = k \cdot \{[\mathrm{CO_2}] - [\mathrm{CO_2}]_e\}$ Design equation derived by integration: $\ln \frac{[\mathrm{CO_2}] - [\mathrm{CO_2}]_e}{[\mathrm{CO_2}]_0 - [\mathrm{CO_2}]_e} = -k \cdot \frac{6(1-\varepsilon)}{d_p \phi} \cdot \frac{L}{u_{app}}$ $6k/\phi$ = 0.03125 mm/s; T = 40°C ε = fractional bed porosity; L = bed length, mm d_p = particle diameter, mm; ϕ = shape factor u_{app} = superficial flow velocity, mm/s
Letterman et al. (1987) [8]	Dissolution by flow of HCl acidified soft water at 9–22°C in four 150–380 mm diameter columns. Packing lengths = 2.1–3.5 m Particle sizes = 9.6–32 mm Initial CO_2 and HCl acidity = 0.002–0.4 mM Superficial velocity = 0.15–12 mm/s Retention time = 230–3800 s	Dissolution assumed to be controlled by mass transfer and a first order surface reaction. Overall rate given by: $R = k \cdot \{[\mathrm{Ca}]_e - [\mathrm{Ca}]\}$ Integration based on dispersion model. Data show that dispersion term is negligible. Form of design equation identical to Yamuchi's except that Ca replaces CO_2. Correlation of k values are given in terms of the Reynolds number.

constant pressure gaseous CO_2 atmosphere, were used by Erga and Terjesen [3], Plummer et al [4,5] and Chan and Rochelle [6]. Dissolution rates were determined by either the free drift method [3] or the more accurate pH-stat method [4–6]. Dissolution in continuous flow of either distilled or soft water over a bed of $CaCO_3$ particles was investigated by Yamauchi et al. [7], Letterman et al. [8] and in this study.

A major difference can be noted in the modeling of the dissolution process. Some authors [3–5,7] assume that the dissolution process is controlled by surface chemical reactions and that diffusional mass transport processes are fast and need not be considered. On the other hand, Chan and Rochelle [5] and Letterman et al. [8] correlate the dissolution data assuming a mass transfer controlled process. A different mass transfer model was adopted in each of these studies.

The most comprehensive investigation is, undoubtedly, that carried out by Plummer et al. [4,5]. The most convenient formulation for limestone bed design is that presented by Yamauchi et al. [7]. According to Yamauchi et al., the basic dissolution rate expression is:

$$R = \frac{Q \cdot d[CO_2]}{dS} = k\left\{[CO_2] - [CO_2]_e\right\} \qquad (21)$$

where Q is the water flow rate and S is surface area of limestone particles. Integration of Eq. (21) gives:

$$-\ln\frac{[CO_2]-[CO_2]_e}{[CO_2]_0-[CO_2]_e} = k\cdot\frac{S_T}{Q} = k\cdot\frac{S_0V(1-\varepsilon)}{Q} = k\cdot\frac{6(1-\varepsilon)}{d_p\phi}\cdot\frac{L}{u_{app}} \qquad (22)$$

where ε is the bed fractional porosity, d_p is the particle size, ϕ is the particle shape factor (ϕ =1 for a sphere, <1 for irregular shapes), L is the bed length and u_{app} is the superficial flow velocity (flow rate/column cross sectional area). Eq. (22) predicts a linear relationship between

$$\ln\frac{[CO_2]-[CO_2]_e}{[CO_2]_0-[CO_2]_e}$$

and the apparent residence time (L/u_{app}). Note that the slope k' of this straight line depends on bed properties (ε, d_p and ϕ).

4. Comparison of dissolution rate correlations

A comparison of results predicted by the various dissolution rate correlations was made by calculating dissolution rates along the dissolution paths of waters having different initial compositions. The dissolution paths examined are shown in Fig. 4. In 6 cases denoted by the letters A–F, dissolution was carried out by distilled water having an initial CO_2 content in the range of 0.005 mM (pH = 5.8) to 16.2 mM (pH = 4.0). In 6 other cases denoted by the letters G–L, dissolution was carried out by soft water having a fixed initial total alkalinity of 3.8 mM and an initial CO_2 content varying from 0.05 mM (pH = 8.15) to 25.0 mM (pH = 5.5).

Fig. 5 shows a comparison of dissolution rates calculated from the correlations of Plummer et al. [4,5] and Yamauchi et al. [7] for a temperature of 40°C along the dissolution paths of the distilled water cases A–F. The initial dissolution rate calculated from Plummer's correlations is much higher than that calculated from Yamauchi's correlation. However, over a considerable medium alkalinity range, there is reasonable agreement in the results evaluated from the two correlations. At very low alkalinities, there is a wider disagreement. Fig 6 shows a similar comparison for the soft water cases G–L. Agreement is mediocre in most cases.

It should be noted that Figs. 5 and 6 are based on differential dissolution rates which accentuate differences. In a practical water remineralization column, the terminal water composition is

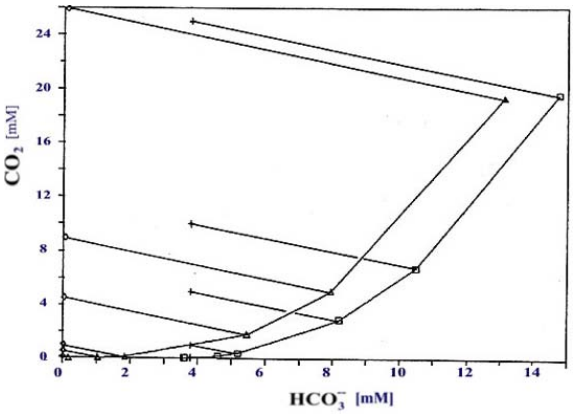

Fig. 4. Dissolution paths in simulation study.

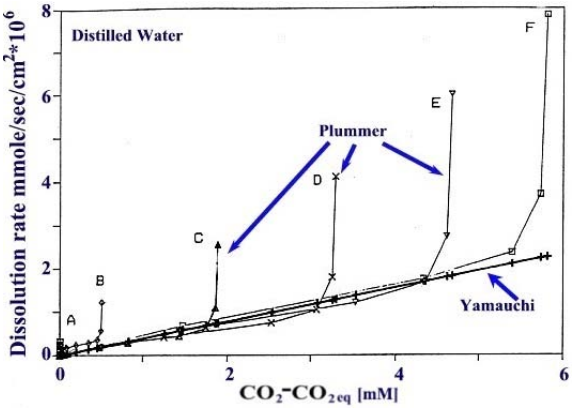

Fig. 5. Comparison of dissolution rates predicted by Yamuchi et al. and Plummer et al. (distilled water simulations).

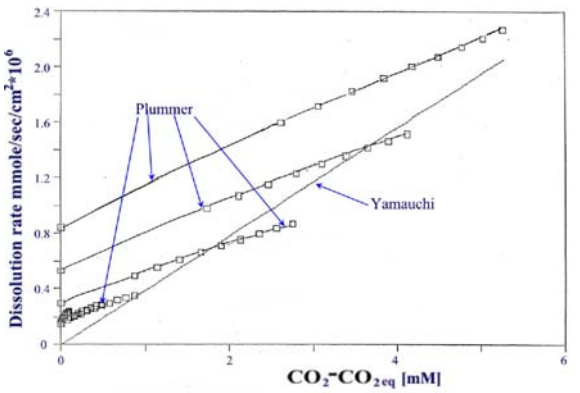

Fig. 6. Comparison of dissolution rates predicted by Yamuchi et al. and Plummer et al. (soft water simulations).

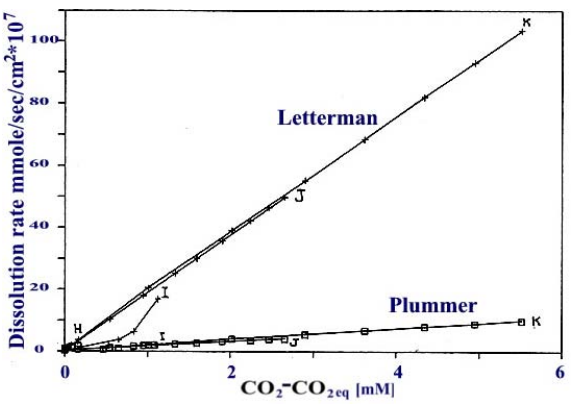

Fig. 7. Comparison of dissolution rates predicted by Plummer et al. and Letterman et al.

governed by integration of the rate equation along the dissolution path. Differences in the exit water composition predicted by the above correlations will be less accentuated. Thus, designs of a remineralization column calculated from the two correlations will give results of the same order of magnitude.

Fig. 7 shows a comparison of dissolution rates calculated from the correlations of Plummer et al. [4,5] and Letterman et al. [8]. Here, there is a very wide discrepancy. The correlation of Letterman et al. predicts considerably higher dissolution rates. Designs based on these two correlations will differ widely.

5. Experimental

In view of the considerable uncertainty in the choice of a rate expression on which to base the design of a remineralization column, an experi-

mental study was carried out to provide first hand dissolution rate data. The functional parts of the experimental system (Fig. 8) were:

- Water supply lines providing either distilled water (prepared by condensing steam) or soft water (prepared by a water softening column)
- A water feed vessel equipped with a stirrer, a thermostatically controlled heating element and a CO_2 gas sparger, connected to pH controlled CO_2 cylinder
- A Perspex column, 32 mm internal diameter, 2 m high, packed with limestone particles (Hydrocarbonat 00 Grade), supplied by Akdolit Co., Germany. Crystallographic analysis confirmed that the particles consisted of pure calcite. Particles were sized by sieving and the fraction in the size range of 2.4–3.4 mm 2.85 mm average) was packed in the column. The limestone particles density was 2640 kg/m^3, bed porosity was 38%, the shape factor of the particles was in the range of 0.6–0.8 and the specific surface of the particles, measured by the pressure drop method, was 4000± 200 m^2/m^3.

The limestone dissolution path along the packed bed was followed by monitoring the composition of water extracted from sampling points located at distances of 14, 34, 64, 104, 170 cm down the column. The pH at the various sampling points was directly read from pH probe inserted in the column wall. Each sample was analyzed to determine its alkalinity and Ca content.

All experiments were carried out at a water temperature of 30 ± 1°C. The nominal water flow rate in the various runs was either 0.1 or 0.2–0.3 L/min, corresponding to superficial velocities of 2, 4.1 and 6.2 mm/s respectively. Since velocity had no apparent effect on the dissolution rate, most runs were carried out at the intermediate flow rate.

Two run series were carried out — Series I with soft water (17 experiments) and Series II with distilled water (7 experiments). The dissolution paths of the various runs are depicted in Fig. 9.

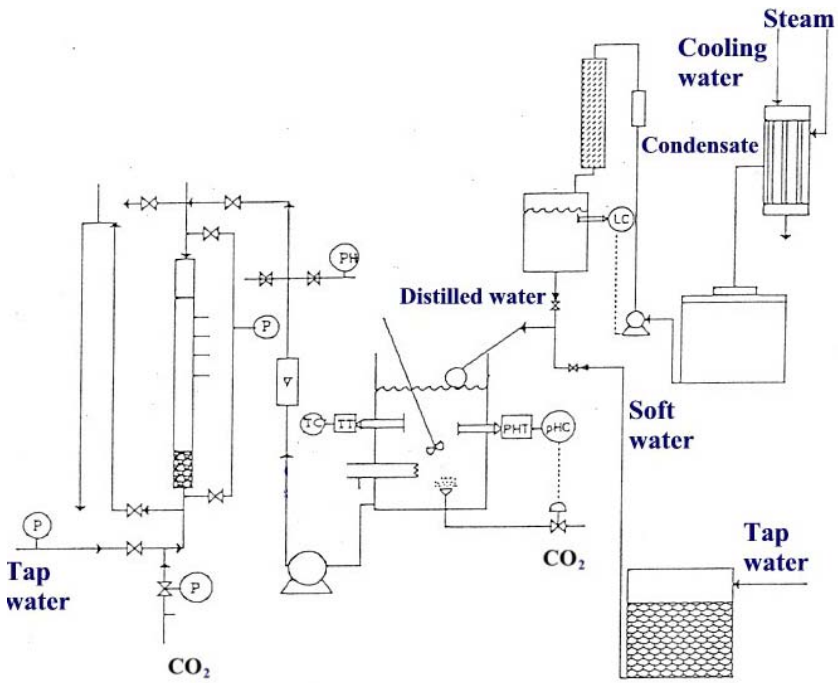

Fig. 8. Experimental system.

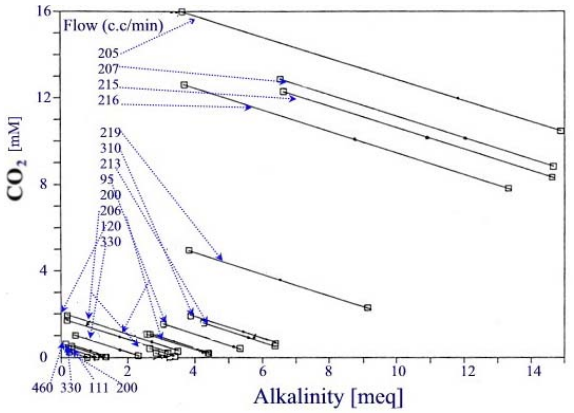

Fig. 9. Dissolution paths of experimental runs.

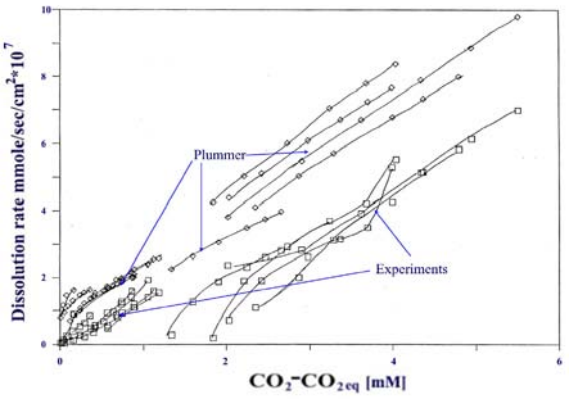

Fig. 10. Comparison of experimental dissolution rates with values predicted by Plummer et al.'s model.

The initial alkalinity in Series I runs varied in the range of 2.6–6.6 meq/L, the initial CO_2 content was in the range of 1.5–15 mM and the initial pH, in the range of 7.3–5.5. In Series II runs, initial alkalinity was in the range of 5–10 meq/L, initial CO_2 content was in the range of 0.5–2 mM and the initial pH, in the range of 6.2–5.2.

6. Results

6.1. Differential analysis of the dissolution rate data

Experimental values of the dissolution rates were obtained by a differential analysis of the composition profile along the length of the column. Fig. 10 compares experimental dissolution rates with dissolution rates predicted by the correlation of Plummer et al. [4,5] as a function of the driving force potential $\{[CO_2] - [CO_2]_e\}$ proposed by Yamauchi et al. [7].

Close examination of the data shows that in runs of high initial CO_2 content $\{[CO_2]_o > 2$ mM or $[CO_2]_o - [CO_2]_e > 0.5$ mM$\}$, the Plummer-predicted dissolution rates are higher by a factor of 3–4 at the inlet region and by a factor of 1.5–2 at the outlet region. In the low CO_2 runs, the deviations are higher and increase progressively with the decrease in CO_2 concentration, reaching deviation factors as high as 10–20.

6.2. Integral analysis of the data

Eq. (22), proposed by Yamauchi el al. [7], enables simple analysis of the experimental data. Plots of

$$\ln\frac{[CO_2]-[CO_2]_e}{[CO_2]_0-[CO_2]_e}$$

vs. column depth L (Fig. 11) displayed the predicted linear relationship, with regression coefficients close to unity. The slope of these straight lines were used to determine values of k', defined by:

$$k' = k\cdot\frac{6(1-\varepsilon)}{d_p\phi} \tag{23}$$

Fig. 12 shows values of the coefficient k' derived from the various runs, plotted as a function of the CO_2 concentration. It is seen that above a CO_2 concentration of 2 mM, the kinetic coefficient is essentially constant, and has the value of $(5.5 \pm 0.5) \times 10^{-3}$ s^{-1}. Inserting values of the bed porosity and particle size, it is found that for dissolutions carried out at 30°C, $6\,k/\phi = 0.025$ mm/s. This result

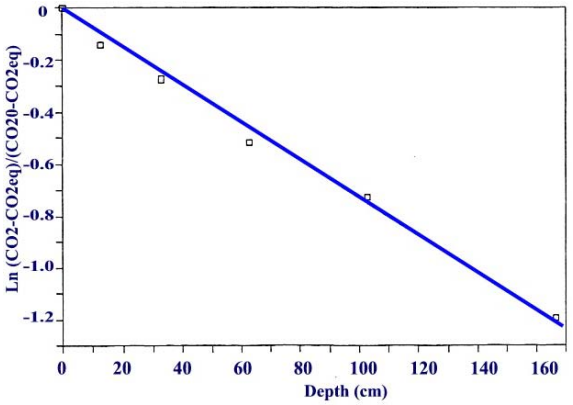

Fig. 11. Linear correlation of the CO_2 depletion along the bed.

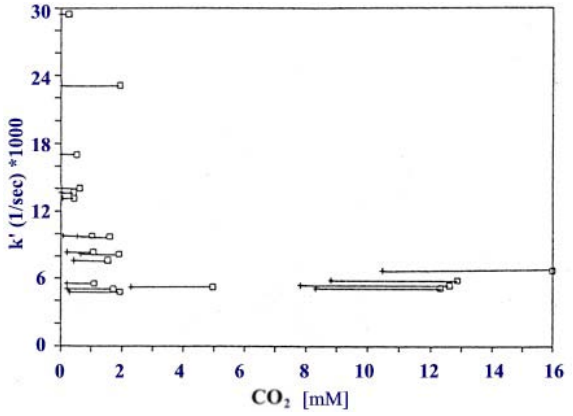

Fig. 12. Effect of the CO_2 concentration on the magnitude of the kinetic coefficient k'.

is in very good agreement with the value $6\,k/\phi$ = 0.025 – 0.031 mm/s measured by Yamauchi et al. at 40°C.

Thus, design of a limestone bed contactor in which the final CO_2 concentration is above 2 mM can be readily designed according to Eq. (22).

Further analysis of the data was carried out in the search of a model which gives a concentration independent kinetic coefficient at CO_2 concentrations below 2 mM. The best results were obtained by adopting the following rate expression:

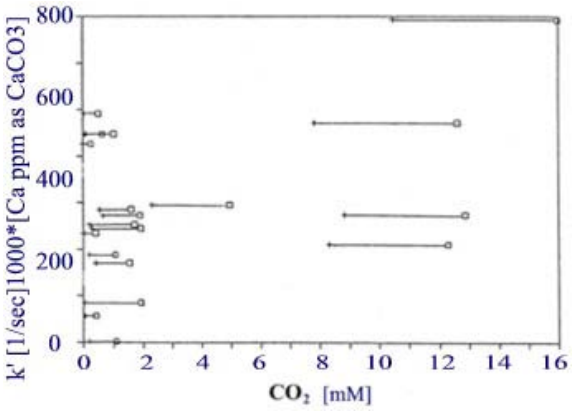

Fig. 13. Effect of the CO_2 concentration on the magnitude of the adjusted kinetic coefficient $k''= k'\cdot[\mathrm{Ca}]_e$.

$$R = \frac{Q\cdot d[\mathrm{CO_2}]}{dS} = k''\frac{\left\{[\mathrm{CO_2}]-[\mathrm{CO_2}]^*\right\}}{[\mathrm{Ca}]_e} \qquad (24)$$

According to this model, $k' = k''/[\mathrm{Ca}]_e$. Hence values of $\{k'\cdot[\mathrm{Ca}]_e\}$ should be independent of concentration. A test of this assumption is shown in Fig. 13. The average value of the kinetic coefficient, based on molar CO_2 concentrations and units of ppm as $CaCO_3$ for Ca_e is:

$$k'' = 0.69 \text{ ppm as } CaCO_3/s \qquad (25)$$

The scatter in the data is moderate, the standard deviation in the value of k'' amounting to 24%. Design of a limestone bed in which the final CO_2 content is well below 2 mM can be made by numerical integration of Eq. (24).

7. Conclusion

Rational design of a limestone bed contactor for remineralizing desalinated water rests on the availability of a reliable kinetic expression relating dissolution rate with water composition. The critical literature review presented in this paper highlights the difficulty that there is substantial

disagreement among the various dissolution models published in the literature.

The results of the present investigation show that a limestone dissolution bed can be simply designed according to Eq. (22) if the terminal CO_2 concentration is sufficiently high. In the low CO_2 concentration region, dissolution rates can be roughly approximated by Eq. (24), which can only be numerically integrated to provide design dimensions.

Further research is called for in order to extend available data, to investigate the effect of temperature and to refine the low CO_2 dissolution rate model.

Acknowledgments

This study was partly supported by the Grand Water Research Institute of the Technion. Thanks are due to Professor Raphael Semiat, Head of the Rabin Desalination Laboratory, for his most useful remarks in reviewing the manuscript of this paper.

References

[1] E Gabbrielli and J.P Gerofi, Appropriate mineral content of desalination water — theory and drinkers' reaction, Desalination, 49 (1984) 95–103.

[2] J.W. Morse, Dissolution kinetics of $CaCO_3$ in sea water. III: A new method for the study of carbonate reaction kinetics, Amer. J. Sci., 274 (1974) 97–107.

[3] O. Erga and S.G. Terjesen, Kinetics of the heterogeneous reaction of calcium bicarbonate formation with special reference to copper ion inhibition, Acta Chim. Scand., 10 (1956) 872–874.

[4] L.N. Plummer, T.M.L. Wigley and D.L. Pakhurst, The kinetics of calcite dissolution in CO_2–water system at 5°C to 60°C and 0.0 to 1.0 atm. CO_2, Amer. J. Sci., 278 (1978) 179–216.

[5] L.N. Plummer and D.L. Pakhurst, Critical review of the kinetics of calcite dissolution and precipitation, ACS Symp. Series, 93 (1979) 538.

[6] P.K. Chan and G.T. Rochelle, Limestone dissolution: effects of pH, CO_2 and buffers modeled by maa transfer, ACS Symp. Series, 97 (1982) 75–97.

[7] Y. Yamauchi, K. Tanaka, K. Hattori, M. Kondo and N. Ukawa, Remineralization of desalinated water by limestone dissolution, Desalination, 60 (1987) 365–383.

[8] R.D. Letterman, C.T. Driscoll, M. Haddad and H.A. Hsu, Limestone bed contactors for control of corrosion at small water utilities, Syracuse University Report, Agreement Cr-809979-01-3 with EPA Office of R&D, 1987, 207 pp.